

GRB 221009A with an unconventional precursor: a typical two-stage collapsar scenario?

XIN-YING SONG ^{1,2} AND SHUANG-NAN ZHANG^{1,2}

¹Key Laboratory of Particle Astrophysics, Institute of High Energy Physics, Chinese Academy of Sciences, Beijing 100049, China

²University of Chinese Academy of Sciences, Chinese Academy of Sciences, Beijing 100049, China

ABSTRACT

As the brightest Gamma-Ray burst (GRB) ever detected, GRB 221009A may offer a chance that reveals some interesting features which are hidden in those bursts that are not so bright. There seems a very weak emission with a flux of $10^{-8} \sim 10^{-7}$ erg cm⁻² s⁻¹ between the first pulse ($T_0 \sim T_0 + 50$ s, T_0 is the trigger time) and the main burst (appears from $T_0 + 180$ s). Thus the gap time between them is not really quiescent, and the first pulse could be taken as an unconventional precursor, which may provide a peculiar case study for the GRB-precursor phenomena. A two-stage collapsar scenario is proposed as the most likely origin for this burst. In this model, the jet for the precursor is produced during the initial core-collapse phase, and should be weak enough not to disrupt the star when it breaks out of the envelope, so that the fallback accretion process and the forming of the disk could continue. We present an approach in which the duration and flux both provide constraints on the luminosity (L_j) and the Lorentz factor at the breakout time (Γ_b) of this weak jet. The estimated $L_j \lesssim 10^{49}$ erg s⁻¹ and Γ_b has an order of ten, which are well consistent with the theoretical prediction. Besides, the weak emission in the gap time could be interpreted as a MHD outflow due to a magnetically driven wind during the period from the proto-neutron star phase to forming the accretion disk in this scenario.

Keywords: gamma-ray bursts:individual–radiation mechanisms: non-thermal

1. INTRODUCTION

Precursors are usual for bright, long GRBs ($\sim 20\%$, e.g., [Lazzati 2005](#)) and the emission types and jet compositions of their precursors and main bursts are listed in Table 1. Quasi-thermal (QT) component could be observed in precursors, as shown in Types 2, 3 and 4, while most of the precursors are found to be non-thermal (NT)(e.g. [Li & Mao 2022](#)). There are some models or mechanisms for precursors of long bursts. Fireball-internal shock (IS) models (e.g., [Mészáros & Rees 2000](#); [Ramirez-Ruiz et al. 2002](#); [Wang & Mészáros 2007](#)) and jet-cocoon interaction (e.g., [Nakar & Piran 2017](#)) both predict a precursor with a quasi-thermal (QT) component, as shown in Types 2, 3 and 4 in Table 1; the quiescent time for the former is estimated to be about 10 s. Jet-cocoon interaction mechanism and the ‘two-stage’ model (e.g., [Cheng & Dai 2001](#); [Wang & Mészáros 2007](#)) both correspond to

a scenario of a collapsar. In the ‘two-stage’ scenario, the precursor is from a weak jet which may be produced by a collapsed core (e.g., [LeBlanc & Wilson jet, LeBlanc & Wilson 1970](#)) or by a rotating proto-neutron star (PNS) during the initial core-collapse phase, while the quiescent time ~ 100 s is the timescale of fallback and forming a proto-compact star with an accretion disk; the central engine of the main burst is a black hole (BH) or neutron star (NS). The process of the ‘two-stage’ model is shown in Figure 1. In the ‘magnetar-switch’ model ([Bernardini et al. 2013](#)), the precursor and the main burst arise from accretion of matter onto the surface of the magnetar; the accretion process can be halted by the centrifugal drag exerted by the rotating magnetosphere onto the infalling matter, allowing for multiple precursors and very long quiescent times. Lipunov’s works (e.g. [Lipunov & Gorbvskoy 2007](#); [Lipunova et al. 2009](#)) suggest a collapsing ‘spinar’ similar to the ‘two-stage’ model, without any accretion in the process. The origins for precursors are still under debate in some works (e.g. [Lazzati 2005](#); [Burlon et al. 2009](#); [Bi et al. 2018](#); [Li & Mao 2022](#)), and it is of importance to perform the precursor research to un-

derstand the physical mechanisms of the GRB central engine.

In this analysis, the so-called precursor in GRB 221009A is not conventional because the ‘quiescent’ time is not really quiescent. Note that in the former works (e.g. [Burlon et al. 2009](#)), a time interval during which the background subtracted light curve is consistent with zero, is defined as a ‘quiescent’ time. For GRB 221009A, there exist some weak emissions between the first pulse ($T_0 \sim T_0 + 50$ s, T_0 is the trigger time) and the main burst beginning at $T_0 + 180$ s, as shown in Figure 2 (a) and (b). However, we still could use the mechanisms for precursors to interpret its origin.

GRB 221009A was detected by many missions, such as Fermi/GBM (GCN 31565, [Lesage & Fermi Gamma-ray Burst Monitor Team 2022](#)), Fermi-LAT (GCN 32637, [Bissaldi et al. 2022](#)), Swift/BAT/XRT (GCN 32632, [Dichiara et al. 2022](#)), Konus-Wind (GCN 31604, [Svinkin et al. 2022](#)), Insight-HXMT (ATel 155660, [Tan et al. 2022](#)), HEBS (GCN 32751, [Liu et al. 2022](#)) and LHAASO (GCN 32677, [Huang et al. 2022](#)). For GRB 221009A, the prompt emission has a long duration ~ 1000 s. The isotropic-equivalent radiated energy $E_{\text{iso},\gamma} \sim 10^{55}$ erg has been reported in some works (e.g., [Frederiks et al. 2023](#); [An et al. 2023](#)). Note that the jet of the main burst is highly collimated with a small opening angle $\theta \sim 1.0^\circ$ ([Ren et al. 2022](#); [An et al. 2023](#)), thus, the outflow has a total energy of $f_b E_{\text{iso}} \sim 10^{51 \sim 52}$ erg with $f_b \sim \theta^2/2$ and $E_{\text{iso}} = E_{\text{iso},\gamma} + E_{\text{iso},k}$, where $E_{\text{iso},k}$ is the isotropic-equivalent kinematic energy and has an order of 10^{55} erg. This is a typical released energy for a collapsar to form a BH or a magnetar (e.g., [MacFadyen et al. 2001](#)), though GRB 221009A is the brightest ever detected in terms of $E_{\text{iso},\gamma}$.

The paper is organized as follows. In Section 2, we extract the observational properties of the first pulse ($T_0 \sim T_0 + 50$ s) and the followed weak emissions ($T_0 + 50$ s $\sim T_0 + 170$ s); in Section 3 several scenarios for the precursor and jet launching are discussed. In Section 4, a conclusion and summary are given based on the discussion.

2. THE OBSERVATIONAL PROPERTIES OF THE FIRST PULSE AND WEAK EMISSIONS

Background (BG) estimation for extremely long GRB 221009A is important. We use the data from nearby orbit as BG for GBM NaI 8 detector, and polynomial with 0-2 orders for GBM BGO 0 detector above 385 keV. The details are shown in Appendix A. As shown in Figure 2 (a) and (b), some weak emissions exist between

the first pulse and the main burst, and are mainly from the lower energy band ($\lesssim 100$ keV). The first pulse lasts ~ 50 s. After a very weak emission with duration of around 70 s, a long bump of 60 s comes before the main burst as shown in Figure 2 (c).

2.1. The first pulse from T_0 to $T_0 + 50$ s

Fittings with BAND, exponential cut-off power law (CPL), and power law (PL) function¹ are performed on the time-integrated spectrum from T_0 to $T_0 + 10$ s which contains 80% photons. The Markov Chain Monte Carlo (MCMC) fitting is performed to find the parameters with the maximum Poisson likelihood. The BAND model is determined to be the best model by the method of bayesian information criterion (BIC, [Wei et al. 2016](#)), and require ΔBIC is at least 6². If with the contribution from HXMT/CsI detectors which have large effective area in high energy region ([Song et al. 2022b](#)), the low energy photon index (α), the high energy photon index (β) and the peak energy (E_p) of νF_ν spectrum is determined to be $\alpha = -1.55 \pm 0.03$, $\beta = -2.02 \pm 0.02$ and $E_p = 242.9 \pm 113.0$ keV as shown in Figure 2 (d). The low photon energy index $\alpha < -2/3$ (the so-called ‘line of death’, [Preece et al. 1998](#)), which is consistent well with the synchrotron mechanism.

The constant cadence (CC, [Burgess 2014](#)) method and Bayesian blocks (BBlocks, [Scargle et al. 2013](#)) method with a false alarm probability $p_0 = 0.01$ are used for binning in time-resolved analysis. We also require the signal-to-noise ratio (S/N) ≥ 30 at least in one detector, so we combine some adjacent bins. The time bins are [0., 1.2], [1.2, 2.4], [2.4, 3.9], [3.9, 6.7], [6.7, 10] s. The evolution of α is shown in Figure 2 (e). Generally, the double-tracking trend of α -flux and E_p -flux, is observed in the first 10 s, which is consistent well with that of one-zone synchrotron model (e.g., [Uhm & Zhang 2014](#); [Li et al. 2019](#)). Note that $\alpha < -1$ for the first pulse, implies non-thermal (NT) emission is dominant. The internal-collision-induced magnetic reconnection and turbulence mechanism (ICMART, [Zhang & Yan 2011](#)) is preferred as the one-zone synchrotron model for this NT emission mainly.

2.2. The weak emissions between the the first pulse and the main burst

The emission from $T_0 + 50$ s to $T_0 + 115$ s has S/N ~ 10 in NaI 8 detector. Therefore, it is difficult to describe

¹ The formulae for spectral models, BAND, CPL, PL could be found in the Appendix in [Song et al. \(2022a\)](#).

² $\Delta\text{BIC} \geq 10$, the preference is very strong; $10 > \Delta\text{BIC} \geq 6$, strong; $6 > \Delta\text{BIC} \geq 2$, positive.

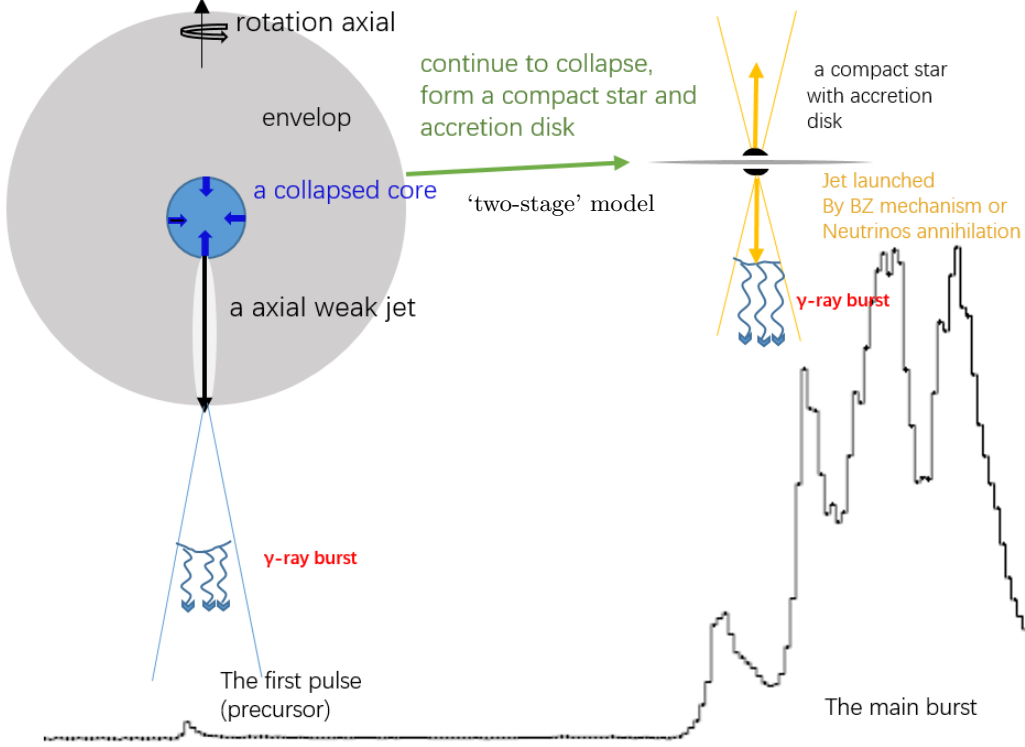


Figure 1. A scenario for the ‘two-stage’ model of precursors.

Table 1. The emission types of long GRBs with precursors. QT: quasi-thermal; NT: non-thermal.

Type No.	1	2	3	4	5
precursor	NT	QT	QT+NT	QT	NT
main burst(or following episodes)	NT	NT	NT	QT+NT	QT+NT

the shape of spectrum. The observed flux is estimated to be $\sim 10^{-8} \text{ erg cm}^{-2} \text{ s}^{-1}$ with PL model as shown in Figure 2 (f). The long bump from $T_0 + 115 \text{ s}$ to $T_0 + 172 \text{ s}$ is best described by CPL function with $\alpha = -1.00 \pm 0.15$ and $E_p = 78.5 \pm 8.0 \text{ keV}$. The flux is $\sim 10^{-7} \text{ erg cm}^{-2} \text{ s}^{-1}$ as shown in Figure 2 (g).

3. THE POSSIBLE ORIGIN OF THE FIRST PULSE

There are some common characteristics between the first pulse in GRB 221009A and the conventional precursor: much weaker than the main burst and a gap time from the main burst. Thus, several models or mechanisms for precursors could be used to interpret origins of the first pulse as well. Fireball-internal shock (IS) models and jet-cocoon interaction are excluded first, because there seems not any evident QT component in the emission of the precursor as discussed in Section 2.1.

Besides, the gap time between the precursor and the main burst is too long ($\sim 100 \text{ s}$) for the fireball-IS model. In the fireball-IS model, the gap time is contributed by three parts (e.g. Wang & Mészáros 2007). The first part (t_1) is the time that the rarefaction wave takes to arrive at the reverse shock. Once the jet head reaches the stellar surface, the pressure in front of the jet head decreases suddenly, and a rarefaction wave will form and propagate back into the shocked jet material at the speed of sound ($c_s = c/\sqrt{3}$). The width of the shocked jet is less than the distance from the core to the envelope (r), thus $t_1 \lesssim r/c_s \simeq 6r_{11} \text{ s}$. The second part (t_2) is from the time that the unshocked jet pass through the envelop, $t_2 = r/c = 3r_{11} \text{ s}$. The internal shock dissipation occurs at about R_d as the beginning

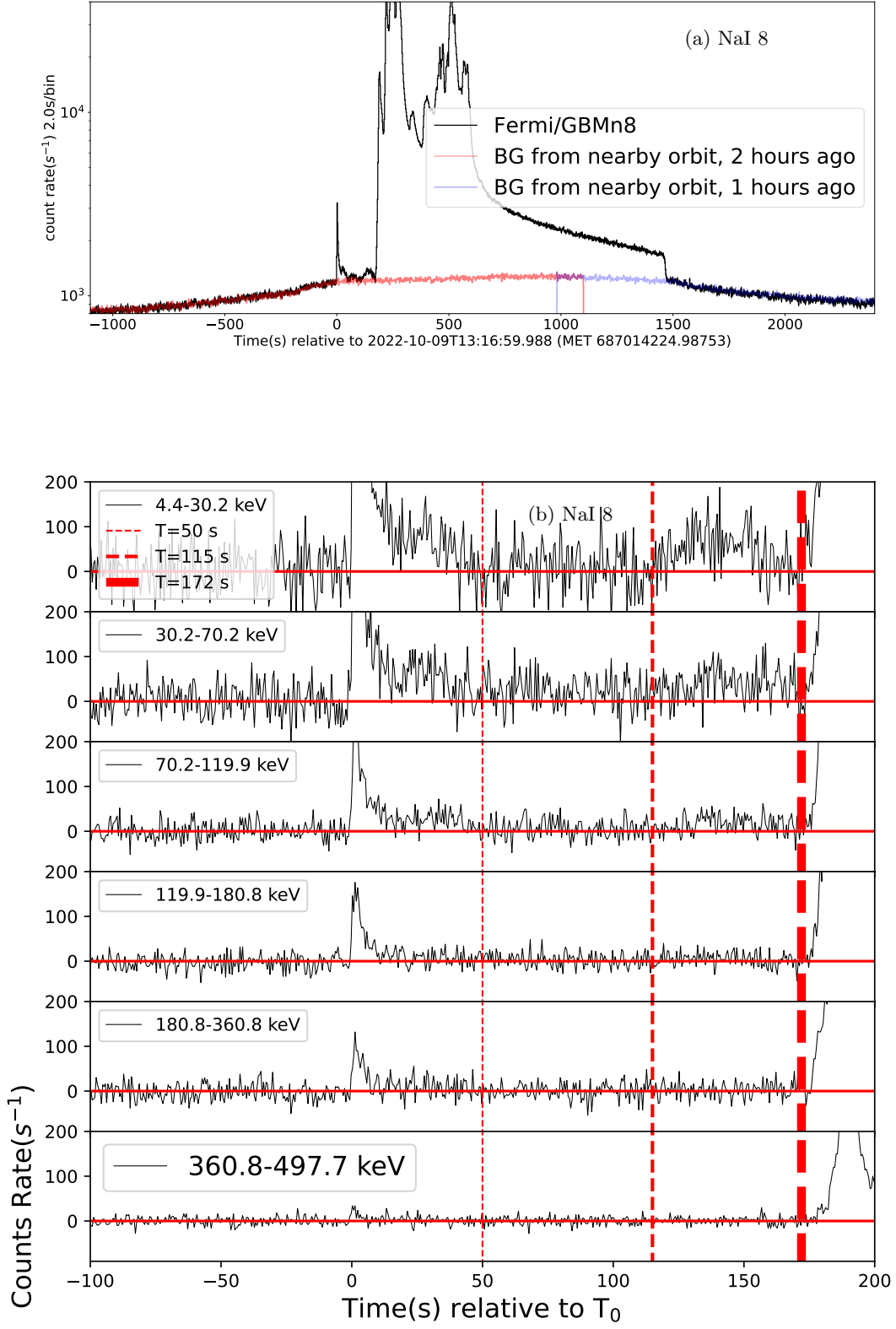


Figure 2. (a) The light curve and BG shape from the data of NaI 8. (b) The BG subtracted light curves in different energy bands of NaI 8. (c) The light curve from T_0 to $T_0 + 200$ s. (d) The spectrum of the first pulse. (e) The light curves from GBM NaI 8 detector and HXMT, α and E_p values of precursor. (f) The spectrum of $T_0 + 50$ s to $T_0 + 115$ s. (g) The spectrum of $T_0 + 115$ s to $T_0 + 172$ s.

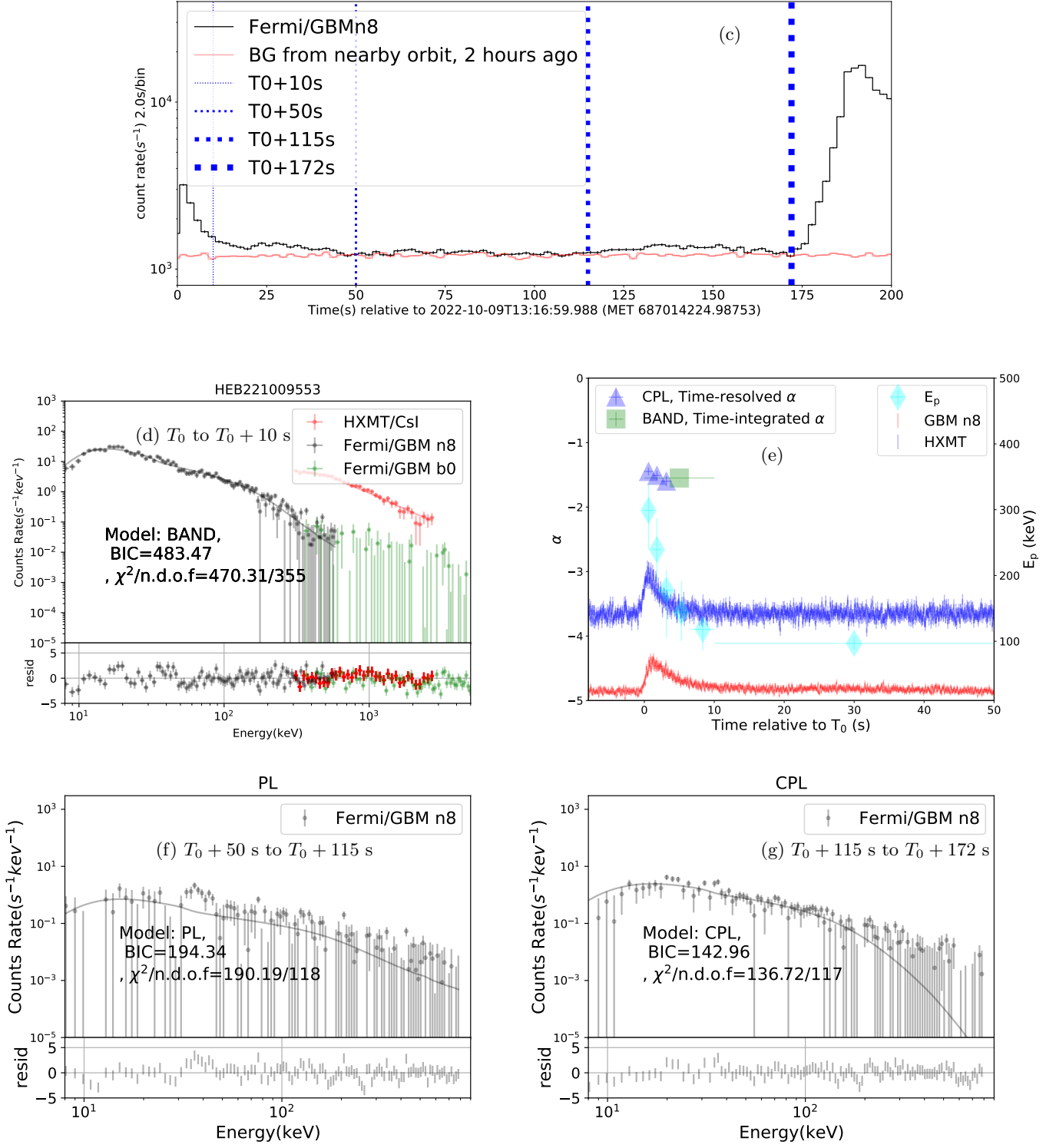


Figure. 2— Continued.

of the main burst, and the third part (t_3) is the delay of the main burst to the precursor, $t_3 = R_d/2\Gamma^2c = 1.7R_{d,15}\Gamma_2^{-2}$ s. The gap time is the sum of t_1 , t_2 and t_3 and has an order of 10 s.

It seems that the ‘two-stage’, ‘magnetar-switch’ and spinar models could be consistent with the NT emission for the precursor and long gap time. Here we define two quantities: (1) the Lorentz factor Γ_b at the breakout time of the jet for the precursor, which is the Lorentz Factor when the jet breaks out of the envelope and can be taken as the maximum Lorentz factor of the jet passing through the envelope;³ (2) the luminosity of the jet (L_j) for the precursor. In the ‘magnetar-switch’ and spinar model, Γ_b and L_j are not constrained especially, while for the two-stage model, the jet for the precursor should be weak enough not to disrupt the star, so that the fallback accretion process and the forming of the disk could continue. In details, a mild $\Gamma_b < 100$ and the released energy $\lesssim 10^{50}$ erg are both required (Wang & Mészáros 2007). Therefore, the estimation of L_j and Γ_b for the first pulse is important. The ‘two-stage’ model can be excluded if a weak jet is not consistent with the data. The first pulse of GRB 221009A has a long duration of tens of seconds (80% photons are in ~ 10 s). Thus, $t_b \lesssim 10$ s, where t_b is the time taken by the jet head to move from the interior of the star to the surface.

Assuming the jet acceleration is saturated, we have Equation (12) in Wang & Mészáros (2007) to describe the relation among Γ_b , L_j and t_b ,

$$\Gamma_b \gtrsim 10r_{11}^{1/2}L_{j,49}^{-1/4}t_{b,10}^{-3/4}, \quad (1)$$

where $r \sim 10^{11}$ cm is the distance from core to envelope; CGS⁴ units are used here. The flux in the first 10 s is $\sim 2 \times 10^{-6}$ erg cm⁻² s⁻¹ ($L_{\text{iso},\gamma} \sim 10^{50}$ erg s⁻¹ with redshift $z = 0.151$ from de Ugarte Postigo et al. (2022); here $L_{\text{iso},\gamma}$ denotes $E_{\text{iso},\gamma}/T$, T is the duration time in the rest frame of central engine; $T = T_{\text{obs}}/(1+z)$ with T_{obs} is that in the rest frame of the observer), thus, the isotropic-equivalent luminosity L_{iso} could be $\gtrsim 10^{50} \sim 10^{51}$ erg s⁻¹ ($L_{\text{iso}} = L_{\text{iso},\gamma}/\epsilon_\gamma$ with radiative efficiency $\epsilon_\gamma \sim 50\% - 90\%$ for ICMART mechanism, Zhang & Yan 2011). Considering the opening angle (θ_b) at the breakout time $\sim 1/\Gamma_b$ and $L_j \sim L_{\text{iso}}\theta_b^2/2$, we have

$$\Gamma_b \sim (2L_j/L_{\text{iso}})^{-1/2}. \quad (2)$$

Here, we present an approach to limit L_j and Γ_b . By combining the above equation and constraint, the region

for the possible values for L_j and Γ_b is the overlap of these two as shown in Figure 3 in dark blue. The range of L_j corresponds to $\lesssim 10^{48}$ erg s⁻¹, and Γ_b has an order of 10, which is consistent well with the weak jet assumption. Note that this estimation is approximate with the orders of magnitudes of these quantities, e.g., $r_{11} \sim 1$ and $L_{\text{iso},51} \sim 1$. For specific values, the order of magnitudes of the results will not be changed much. If we use the full time of the first pulse, $t_b \lesssim 50$ s, the edge of the violet shadow in Figure 3 which denotes the lower limit of the Γ_b will move to the lower range according to Constraint (1); $L_{\text{iso},\gamma} \sim 2.5 \times 10^{49}$ erg s⁻¹ is smaller, thus the possible Γ_b and L_j become much smaller than those with $t_b \lesssim 10$ s.

For the unsaturated acceleration case, as already calculated in Equation (11) in Wang & Mészáros (2007) for $t_b \lesssim 10$ s, $\Gamma_b \gtrsim 10$. In this case, the upper limit of $\theta_b \lesssim 0.1$, so that $L_j \sim L_{\text{iso}}\theta_b^2/2$ is still weak with luminosity of $10^{48} \sim 10^{49}$ erg s⁻¹, since $L_{\text{iso}} \sim 10^{50} - 10^{51}$ erg s⁻¹.

Therefore, from the above discussion, the observed flux and duration of this pulse both provide constraints on $L_j \lesssim 10^{49}$ erg s⁻¹ in this case. Otherwise, a shorter duration or larger luminosity could result in a larger Γ_b or L_j , so that the assumption of a weak jet fails. Note that the estimated θ_b is not small and the weak jet from the initial collapsar is an axial jet (e.g., LeBlanc & Wilson 1970); the strong jet of the main burst launched by, e.g. the Blandford–Znajek (BZ) mechanism (Blandford & Znajek 1977), is also in the axial direction of rotation, thus, we still could see the burst with the first pulse, though the latter is highly collimated with a much smaller opening angle.

One question arises that there may be a possible jet-cocoon interaction during the jet passing through the envelop. If Γ_b is large enough, the mixing between the two components (the jet material and a stellar material shocked by the expanding high pressure cocoon) could be ignored. As simulated numerically in Nakar & Piran (2017), a relativistic cocoon may produce a short (a few seconds) extremely bright QT burst (with the observed temperature of 10–100 keV) as the precursor. Otherwise, if Γ_b is small enough, the partial mixing occurs (Nakar & Piran 2017). As a result, optical/UV emission should appear with temperature of $\sim 10^4$ K, beyond the observed precursor phase; unfortunately, the optical/UV observations started much later and can not offer more information on this. There is no evident thermal component observed in the precursor, furthermore, most of

³ Note that Γ_b may be not the maximum Lorentz Factor of the jet (Γ) and $\Gamma_b < \Gamma$;

⁴ the convention $Q = 10^n Q_n$ is adopted for CGS units.

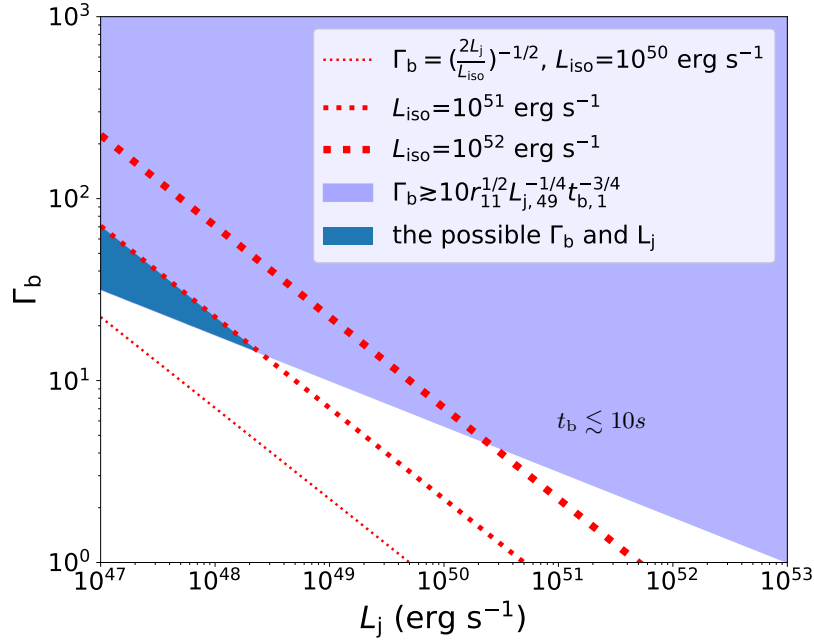


Figure 3. The relation between Γ_b and L_j in Equation (2) in red dotted lines of different L_{iso} . The violet shadow denotes the possible $\Gamma_b - L_j$ only with the Constraint (1) if $t_b \lesssim 10$ s. The dark blue shadow denotes the region of possible Γ_b and L_j .

emission in the precursor is NT at least. This might be also evidence that the jet responsible for the precursor is weak with a mild Lorentz Factor.

Another constraint for the origin is the weak emission between the first pulse and the huge main burst. As estimated in Section 2.1, the flux of the weak emission has an order of $10^{-8} \sim 10^{-7} \text{ erg cm}^{-2} \text{ s}^{-1}$, which is one to two magnitudes smaller than that of the first pulse ($\sim 10^{-6} \text{ erg cm}^{-2} \text{ s}^{-1}$). In a collapsar scenario of the ‘two-stage’ model, the ‘quiescent’ time is the time scale of the period from the PNS phase to forming an accretion disk. During this time, the newborn NS would launch a strong neutrino-driven wind, or a magnetically driven wind due to the differential rotation of the NS. A semi-analytical spindown formula (Siegel et al. 2014) for a magnetically driven wind gives a luminosity of

$$L \simeq 10^{48} B_{14}^2 R_6^3 P_{-4}^{-1} \text{ erg s}^{-1}, \quad (3)$$

where B is the surface magnetic field strength at the polar cap region, R is the radius of the NS, and P is the period. It seems that this spindown mechanism could produce a MHD outflow with luminosity of one to two magnitudes smaller than that of the first pulse ($\sim 10^{49} \text{ erg s}^{-1}$) if the values of B , R and P are in reasonable ranges.

For the ‘magnetar-switch’ model, the longer the waiting time, the higher the stored energy available for the

next emission episode. The ‘quiescent’ time for GRB 221009A is long, and the main burst is extremely bright, which seems consistent with the prediction of ‘magnetar-switch’. There are three mechanisms of energy extraction for a magnetar as a central engine for a GRB, including 1) spin down controlled by magnetic dipole radiation, 2) extracting differential rotational energy of the NS through an erupting magnetic bubbles by winding up the poloidal magnetic field into the a toroidal configuration (Kluźniak & Ruderman 1998), and 3) accretion. **In the propeller mechanism, the accretion process can be halted by the centrifugal drag exerted by the rotating magnetosphere onto the infalling matter, and during the halting time, there should be no evident emission emitted. The weak emission of 60 s before the main burst is not predicted in this model. If ‘magnetar-switch’ works, it is necessary to interpret the long bump of 60 s before the main burst at least. If we assume it is not from the beginning of the re-accretion, it must be from the magnetic dipole radiation or the erupting magnetic bubbles. The former should exist during the burst and does not begin at $T_0 + 112$ s; the latter occurs at a hot PNS phase, and the released energy ($\sim 10^{51} \text{ erg}$) seems too high for the bump. If it is the beginning of the re-accretion, it is not reasonable that it lasts ~ 60 s with a very low luminos-**

ity ($\sim 10^{49} \text{ erg s}^{-1}$, corresponding to $\sim 10^{-7} \text{ erg cm}^{-2} \text{ s}^{-1}$ at the distance of this GRB) as the next emission episode with high energy. Moreover, the magnetar-switch scenario offers a good explanation for these GRBs whose precursors have spectral and temporal properties similar to the main prompt emission, and smaller, but comparable, energetics (Bernardini et al. 2013), because the origins for precursors and main bursts are the same in this model. It is significant that the energies released in precursor and the main emission are not comparable for GRB 221009A. Therefore, considering these inconsistencies, the ‘magnetar-switch’ model may be not the best interpretation for GRB 221009A.

In the scenario of the spinar model, the details for a weak jet corresponding to the precursor are not predicted or constrained. It also occurs in a collapsar scenario, thus we think the production of the long bump may be similar to that in two-stage model. There is not enough information for us to rule out or accept it. Table 2 is a summary of the consistency between the mechanisms for GRB precursors and the observational properties of GRB 221009A. If one property could be interpreted or predicted by the mechanism, the corresponding blank in the table is filled with ‘Yes’; otherwise, ‘No’ is filled for the inconsistency, and ‘?’ is for the case of no prediction. **For example, the weak jet is not predicted in the spinar model, thus the blank is filled with ‘?’.**

In general, from the analysis of the first pulse or precursor and the ‘quiescent’ time, it is proposed that the properties of the first pulse are well consistent with the prediction by mechanism for the precursor in the ‘two-stage’ model in the collapsar scenario. Moreover, the first pulse is different from the traditional definition of the precursor because of the weak emission in the gap time.

4. DISCUSSION AND SUMMARY

We present an approach to infer the possible ranges of Γ_b and L_j of the jet for the first pulse with the constraints from the duration and flux in a collapsar sce-

nario. Furthermore, this approach could be used to speculate the origins of the precursors of GRBs in the future study.

The first pulse of GRB 221009A is non-thermal, which is the difference between GRB 221009A and GRB 160625B (e.g., Zhang et al. 2018); the first precursor of the latter is dominated by a thermal component. In the scenario of GRB 160625B, the precursor occurs after the formation of the accretion disk. As a comparison, we consider that for GRB 221009A the precursor is from the weak jet produced by a rotating PNS during the initial core-collapse phase, rather than the initial prompt accretion phase, as shown in Figure 1. Considering the estimated luminosity ($\lesssim 10^{49} \text{ erg s}^{-1}$) with duration of tens of seconds, the total energy ($\sim 10^{50} \text{ erg}$) the jet carried is well consistent with that predicted by e.g. LeBlanc & Wilson (1970); Wheeler et al. (2000). In summary, the origin for the first pulse is discussed conservatively in this analysis, and a weak jet from the initial core-collapse phase in the ‘two-stage’ scenario is taken as the most likely origin, while the other origin for the precursor, the spinar model, is not ruled out.

As the brightest GRB ever detected, GRB 221009A may provide a case that reveals some interesting features which are hidden in those bursts that are not so bright. If the source of the burst had a high z , or the observations were not so head-on, the weak emission in the gap time might be missed in the detection. In that case, the gap time seems quiescent and the first pulse should seem similar to the precursors detected before. However, in GRB 221009A, a weak emission during the gap time is observed which enriches the GRB-precursor phenomena, and is important for us to understand the physical mechanisms of the GRB central engine.

- 1 The authors thank supports from the National
- 2 Program on Key Research and Development
- 3 Project (2021YFA0718500). This work was par-
- 4 tially supported by International Partnership Pro-
- 5 gram of Chinese Academy of Sciences (Grant
- 6 No.113111KYSB20190020). The authors are very grate-
- 7 ful to the GRB data of Fermi/GBM, HXMT and HEBS
- 8 and konus-Wind. We are very grateful for the com-
- 9 ments and suggestions of the anonymous referees. Dr.
- 10 Xin-Ying Song thanks Dr Ming-Yu Ge and Dr Yuan
- 11 You for the suggestions on the background estimation.

APPENDIX

Table 2. The consistency between the mechanisms for precursors and GRB 221009A.

GRB 221009A/mechanisms for precursors	fireball-IS	jet-cocoon interaction	two-stage	magnetar-switch	spinar
Long gap time(~ 100 s)	No	Yes	Yes	Yes	Yes
NT precursor	No	No	Yes	Yes	Yes
The jet corresponding to precursor is weak enough	No	No	Yes	No	?
The long bump (~ 60 s, 10^{-7} erg cm $^{-2}$ s $^{-1}$) before the main burst	No	No	Yes	No	?

A. ABOUT BACKGROUND ESTIMATION

The background (BG) estimation for extremely long GRB 221009A is important. Figure 4 shows the events data from the nearby orbits, which helps us know the shape of BG. The shift time (~ 5720 s) is determined by the smallest sum of squares of the difference between the two light curves from $T_0 - 1000$ s to T_0 from GRB 221009A and nearby orbit. Figure 5 shows the light curves and events data from the nearby orbit as BG in different energy bands. The BG could be well described by the data from nearby orbits for NaI 7 and 8 detectors. However, from Figure 4 (c) and 5 (c) for BGO data, the nearby data are not very consistent with those from trigger of GRB 221009A. From above 385 keV, we find the the GRB events ends at ~ 600 s. Therefore, we could use a polynomial to describe $T_0 + [-1100, -5]$ s and $[900, 2400]$ s, so that the peaking structure could be well described. The contribution below 385.2 keV in BGO 0 (channels 0-5) is ignored in the fitting procedure.

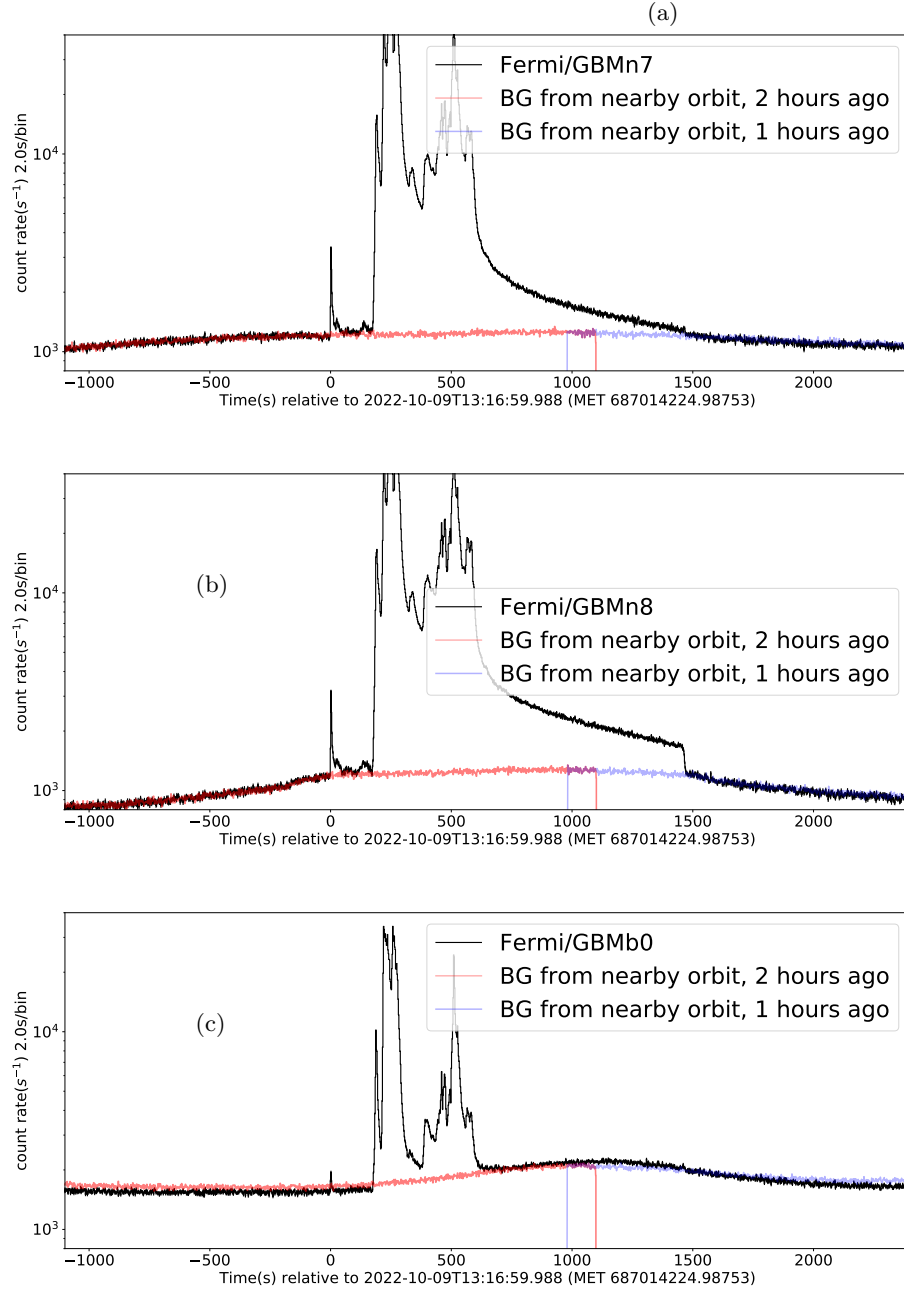


Figure 4. The light curves of BGO, NaI 7 and NaI 8 from $T_0 - 1100$ s to $T_0 + 2500$ s and nearby orbits.

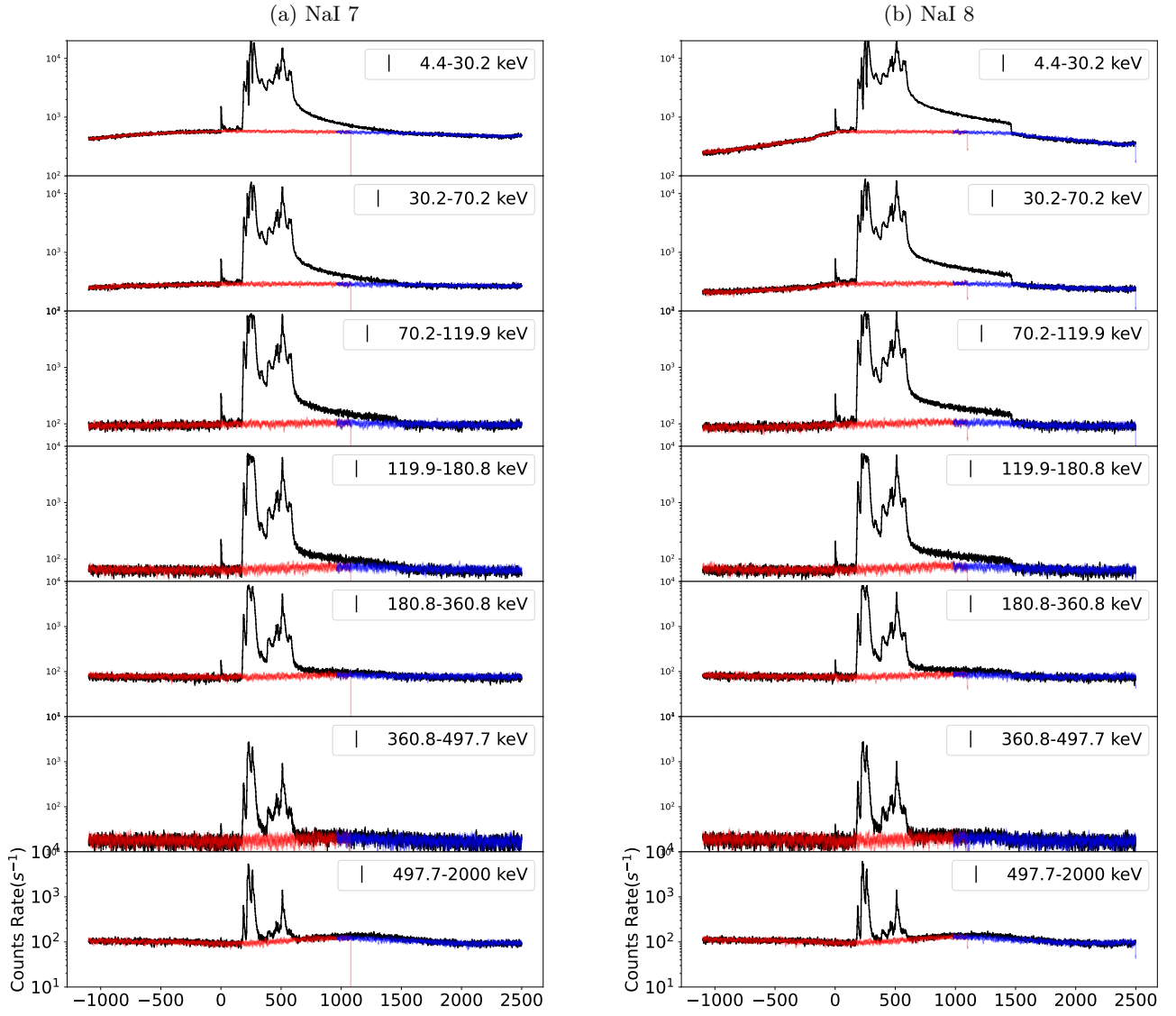


Figure 5. The light curves of NaI 7, 8 and BGO 0 from $T_0 - 1100$ s to $T_0 + 2500$ s and nearby orbits in different energy bands.

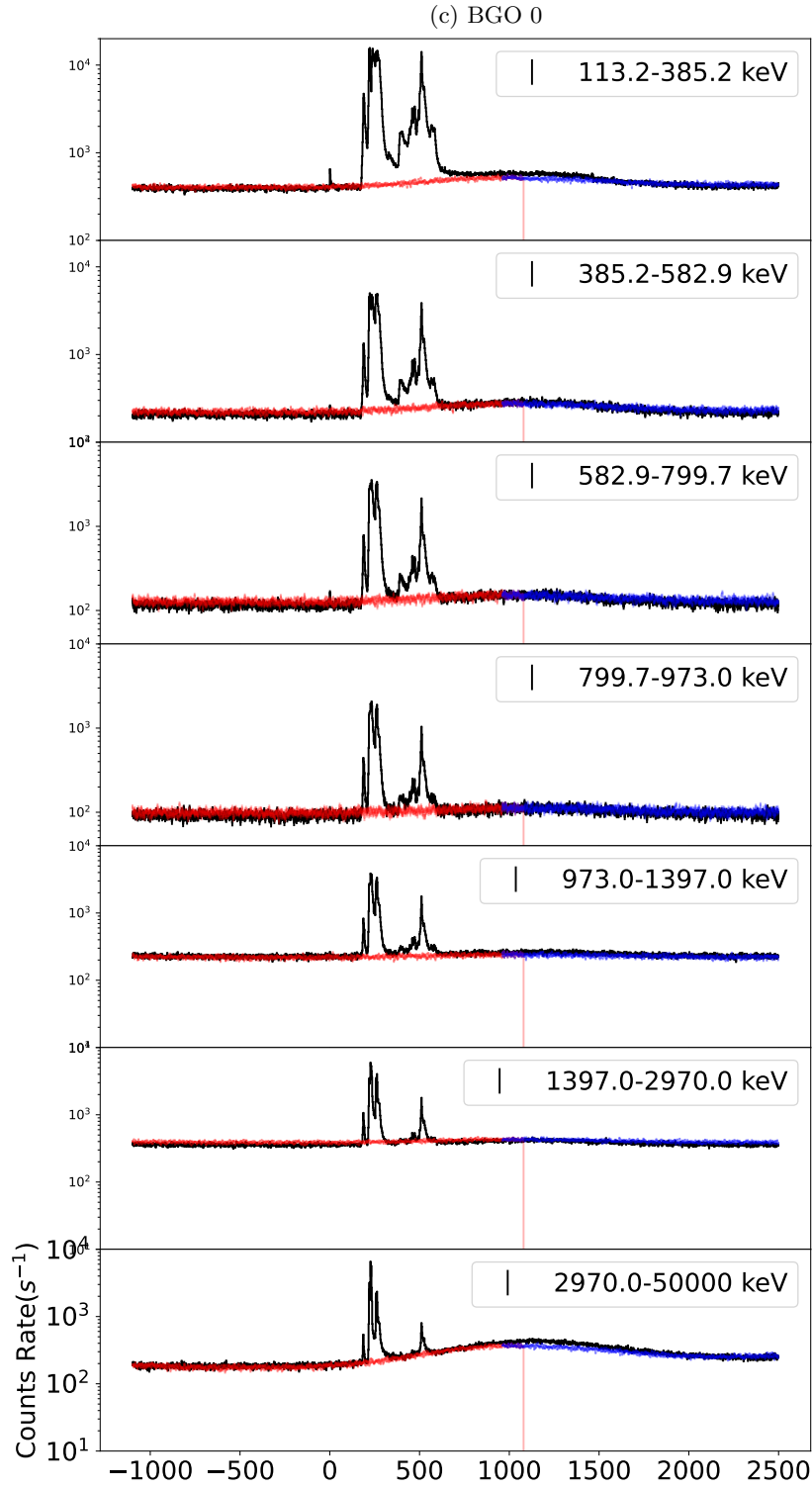


Figure. 5— Continued.

REFERENCES

- An, Z.-H., Antier, S., Bi, X.-Z., et al. 2023, <https://arxiv.org/abs/2303.01203>
- Bernardini, M. G., Campana, S., Ghisellini, G., et al. 2013, *ApJ*, 775, 67, doi: [10.1088/0004-637X/775/1/67](https://doi.org/10.1088/0004-637X/775/1/67)
- Bi, X., Mao, J., Liu, C., & Bai, J.-M. 2018, *ApJ*, 866, 97, doi: [10.3847/1538-4357/aadcf8](https://doi.org/10.3847/1538-4357/aadcf8)
- Bissaldi, E., Omodei, N., Kerr, M., & Fermi-LAT Team. 2022, GRB Coordinates Network, 32637, 1
- Blandford, R. D., & Znajek, R. L. 1977, *MNRAS*, 179, 433, doi: [10.1093/mnras/179.3.433](https://doi.org/10.1093/mnras/179.3.433)
- Burgess, J. M. 2014, *MNRAS*, 445, 2589, doi: [10.1093/mnras/stu1925](https://doi.org/10.1093/mnras/stu1925)
- Burlon, D., Ghirlanda, G., Ghisellini, G., Greiner, J., & Celotti, A. 2009, *A&A*, 505, 569, doi: [10.1051/0004-6361/200912662](https://doi.org/10.1051/0004-6361/200912662)
- Cheng, K. S., & Dai, Z. G. 2001, *Astroparticle Physics*, 16, 67, doi: [10.1016/S0927-6505\(00\)00172-9](https://doi.org/10.1016/S0927-6505(00)00172-9)
- de Ugarte Postigo, A., Izzo, L., Pugliese, G., et al. 2022, GRB Coordinates Network, 32648, 1
- Dichiara, S., Gropp, J. D., Kennea, J. A., et al. 2022, GRB Coordinates Network, 32632, 1
- Frederiks, D., Svinkin, D., Lysenko, A. L., et al. 2023, arXiv e-prints, arXiv:2302.13383, doi: [10.48550/arXiv.2302.13383](https://doi.org/10.48550/arXiv.2302.13383)
- Huang, Y., Hu, S., Chen, S., et al. 2022, GRB Coordinates Network, 32677, 1
- Kluźniak, W., & Ruderman, M. 1998, *ApJL*, 505, L113, doi: [10.1086/311622](https://doi.org/10.1086/311622)
- Lazzati, D. 2005, *MNRAS*, 357, 722, doi: [10.1111/j.1365-2966.2005.08687.x](https://doi.org/10.1111/j.1365-2966.2005.08687.x)
- LeBlanc, J. M., & Wilson, J. R. 1970, *ApJ*, 161, 541, doi: [10.1086/150558](https://doi.org/10.1086/150558)
- Lesage, S., & Fermi Gamma-ray Burst Monitor Team. 2022, GRB Coordinates Network, 31565, 1
- Li, L., & Mao, J. 2022, *ApJ*, 928, 152, doi: [10.3847/1538-4357/ac4af2](https://doi.org/10.3847/1538-4357/ac4af2)
- Li, L., Geng, J.-J., Meng, Y.-Z., et al. 2019, *ApJ*, 884, 109, doi: [10.3847/1538-4357/ab40b9](https://doi.org/10.3847/1538-4357/ab40b9)
- Lipunov, V., & Gorbvskoy, E. 2007, *ApJL*, 665, L97, doi: [10.1086/521099](https://doi.org/10.1086/521099)
- Lipunova, G. V., Gorbvskoy, E. S., Bogomazov, A. I., & Lipunov, V. M. 2009, *MNRAS*, 397, 1695, doi: [10.1111/j.1365-2966.2009.15079.x](https://doi.org/10.1111/j.1365-2966.2009.15079.x)
- Liu, J. C., Zhang, Y. Q., Xiong, S. L., et al. 2022, GRB Coordinates Network, 32751, 1
- MacFadyen, A. I., Woosley, S. E., & Heger, A. 2001, *ApJ*, 550, 410, doi: [10.1086/319698](https://doi.org/10.1086/319698)
- Mészáros, P., & Rees, M. J. 2000, *ApJ*, 530, 292, doi: [10.1086/308371](https://doi.org/10.1086/308371)
- Nakar, E., & Piran, T. 2017, *ApJ*, 834, 28, doi: [10.3847/1538-4357/834/1/28](https://doi.org/10.3847/1538-4357/834/1/28)
- Preece, R. D., Briggs, M. S., Mallozzi, R. S., et al. 1998, *ApJL*, 506, L23, doi: [10.1086/311644](https://doi.org/10.1086/311644)
- Ramirez-Ruiz, E., MacFadyen, A. I., & Lazzati, D. 2002, *MNRAS*, 331, 197, doi: [10.1046/j.1365-8711.2002.05176.x](https://doi.org/10.1046/j.1365-8711.2002.05176.x)
- Ren, J., Wang, Y., & Zhang, L.-L. 2022, arXiv e-prints, arXiv:2210.10673, doi: [10.48550/arXiv.2210.10673](https://doi.org/10.48550/arXiv.2210.10673)
- Scargle, J. D., Norris, J. P., Jackson, B., & Chiang, J. 2013, *ApJ*, 764, 167, doi: [10.1088/0004-637X/764/2/167](https://doi.org/10.1088/0004-637X/764/2/167)
- Siegel, D. M., Ciolfi, R., & Rezzolla, L. 2014, *ApJL*, 785, L6, doi: [10.1088/2041-8205/785/1/L6](https://doi.org/10.1088/2041-8205/785/1/L6)
- Song, X.-Y., Zhang, S.-N., Ge, M.-Y., & Zhang, S. 2022a, *MNRAS*, 517, 2088, doi: [10.1093/mnras/stac2764](https://doi.org/10.1093/mnras/stac2764)
- Song, X.-Y., Xiong, S.-L., Zhang, S.-N., et al. 2022b, *ApJ*, 259, 46, doi: [10.3847/1538-4365/ac4d22](https://doi.org/10.3847/1538-4365/ac4d22)
- Svinkin, D., Frederiks, D., Ulanov, M., et al. 2022, GRB Coordinates Network, 31604, 1
- Tan, W. J., Li, C. K., Ge, M. Y., et al. 2022, *The Astronomer's Telegram*, 15660, 1
- Uhm, Z. L., & Zhang, B. 2014, *Nature Physics*, 10, 351, doi: [10.1038/nphys2932](https://doi.org/10.1038/nphys2932)
- Wang, X.-Y., & Mészáros, P. 2007, *ApJ*, 670, 1247, doi: [10.1086/522820](https://doi.org/10.1086/522820)
- Wei, J.-J., Wu, X.-F., & Melia, F. 2016, *MNRAS*, 463, 1144, doi: [10.1093/mnras/stw2057](https://doi.org/10.1093/mnras/stw2057)
- Wheeler, J. C., Yi, I., Höflich, P., & Wang, L. 2000, *ApJ*, 537, 810, doi: [10.1086/309055](https://doi.org/10.1086/309055)
- Zhang, B., & Yan, H. 2011, *ApJ*, 726, 90, doi: [10.1088/0004-637X/726/2/90](https://doi.org/10.1088/0004-637X/726/2/90)
- Zhang, B. B., Zhang, B., Castro-Tirado, A. J., et al. 2018, *Nature Astronomy*, 2, 69, doi: [10.1038/s41550-017-0309-8](https://doi.org/10.1038/s41550-017-0309-8)